International Cartographic Association
Association Cartographique Internationale

Development of an adaptive TDCP and RTK/INS tightly coupled navigation system for autonomous vehicles

Shuai Guo [a], Hongzhou Yang [a,*], Yang Gao [a]

[a] *Department of Geomatic Engineering, University of Calgary, shuai.guo@ucalgary.ca, honyang@ucalgary.ca, ygao@ucalgary.ca*

* Corresponding author

Abstract: Autonomous vehicle technologies are useful for unmanned ground vehicles, mobile robotics, micro-air vehicles, and logistics which become one of the key research points in recent years. Real-Time Kinematic/Inertial Navigation System (RTK/INS) tightly coupled systems are widely used in navigation systems. They use complementary information of Global Navigation Satellite System (GNSS) and INS to provide continuous and robust positioning and navigation solutions in various application scenarios. In this paper, we extend time-differenced carrier phase (TDCP) in RTK/INS tightly coupled algorithm to achieve low-power consumption navigation system, which can aid autonomous vehicles getting high accuracy position. In conventional RTK/INS tightly coupled systems, the pseudorange, Doppler, and carrier phase of GNSS are used to integrate with INS complementarily, which has high power consumption. Because the sampling rate of Inertial Measurement Unit (IMU) is usually around hundreds of hertz and the RTK/INS tightly coupled algorithm is complicated. Unlike conventional RTK/INS tightly coupled system, this system adaptively utilizes TDCP positioning module to work independently at lower sample rates and simple structure getting high-precision position in some good condition like open-sky. RTK/INS tightly coupled module will stop work at this time to save power consumption and computation. In addition, considering the positioning error of TDCP will drifting, this system will adaptively use RTK/INS tightly coupled module to correct the drifting error of TDCP periodically to help system maintain high-precision navigation continuously. Experimental results show the positioning error of TDCP remained within relatively acceptable bounds for general navigation scenarios despite the drift. The maximum errors over 30 minutes in east, north, and up direction are around 0.333 m, -0.446 m, and 3.598 m, respectively. Besides, RMS significantly decreases with calibration by RTK/INS tightly coupled system compared to cases without calibration, which demonstrates the effectiveness of periodic correction in mitigating cumulative drift for TDCP.

Keywords: autonomous vehicles, RTK/INS tightly coupled, TDCP, high-precision, low-power consumption

1. Introduction

The rapid advancement of autonomous vehicle technology has created an urgent demand for highly reliable and precise navigation systems, particularly in challenging environments (Van et al., 2018). Global Navigation Satellite System (GNSS) technology is a very effective way to get accurate position, which is critical for the navigation of autonomous vehicles (Hegarty and Chatre, 2009).

Real-Time Kinematic (RTK) positioning is widely adopted for positioning tasks requiring higher accuracy. Since RTK requires a fixed base station or access to a continuously operating reference station (CORS) network (Zeybek, 2021). It may not always be available, particularly in remote areas. Its accuracy also degrades with increase of distance from the base station due to the growing impact of atmospheric and signal propagation errors (Feng and Wang, 2008). In addition, in challenging environments, GNSS signals encounter significant challenges, including the number of visible satellites, multipath and none-line-of-sight (NLOS), signal attenuation, and interference from buildings (Tokura and Kubo, 2016). A feasible solution is to integrate the data from other sensors, like the Inertial Navigation Systems (INS).

RTK/INS tightly coupled system can mitigate these problems in some certain. In the conventional RTK/INS tightly coupled algorithm, the pseudo-range, Doppler, and carrier phase generated from the GNSS receiver are used to form the Kalman Filter (KF) measurement equation. It offers superior positioning accuracy while introducing several significant technical challenges like complex system architecture, high computational demands, and excessive power consumption.

Time-differenced carrier phase (TDCP) can provide precise relative positioning since it does not rely on fixed base station or external correction services as the case in RTK techniques (Soon et al., 2008). By differencing the GNSS carrier phase measurements over time (Li et al., 2022), the TDCP-based technique can cancel out the ionospheric delay, tropospheric delay, satellite clocks and orbit errors. This algorithm has been applied to estimate the velocity with high accuracy (Suzuki, 2022). While TDCP techniques offer improved short-term stability compared to standalone GNSS, they remain susceptible to cumulative error drift over extended periods, limiting their effectiveness for long-duration autonomous operations.

To address these limitations, this paper presents the development of a tightly coupled RTK/INS-aided TDCP navigation system, designed to deliver low power assumption and high-precision positioning in GNSS-challenged scenarios. By integrating RTK's centimeter-level accuracy, INS's high-rate motion tracking, and TDCP's resistance to cycle slips, the tightly coupled architecture enables real-time sensor fusion, leveraging Kalman filtering to optimally estimate and correct errors across all subsystems. The results suggest that while TDCP alone provides reasonably accurate positioning, integrating periodic correction significantly refines performance, particularly in environments where error accumulation would otherwise degrade precision over time. This approach not only improves positioning consistency but also supports energy-efficient navigation by reducing the need for excessive computational corrections.

2. Methodology

2.1 TDCP measurement model

The carrier phase measurements model can be written as follows:

$$\phi = \frac{1}{\lambda}\left(\rho_u^s + cdt_u - cdt^s - I_\phi + T_\phi\right) + N + \varepsilon_\phi \tag{1}$$

where ϕ is the carrier phase measurement in cycles, λ is the carrier wavelength, ρ_u^s is the geometric range between the satellite and the receiver antenna, c is the speed of light in a vacuum, dt_u is the receiver clock bias, dt^s is the satellite clock bias, I_ϕ is the ionospheric delay, T_ϕ is the tropospheric delay, N is the carrier phase integer ambiguity in cycles, ε_ϕ is the measurement errors of carrier phase.

The carrier phase measurement equation at epoch t_k can also be expressed as follows:

$$\begin{aligned}\phi(t_k) &= \frac{1}{\lambda}\left[\rho_u^s(t_k) + cdt_u(t_k) - cdt^s(t_k)\right] + \\ &\frac{1}{\lambda}\left[-I_\phi(t_k) + T_\phi(t_k)\right] + N(t_k) + \varepsilon_\phi(t_k)\end{aligned} \tag{2}$$

Similarly, the carrier phase measurement equation at epoch t_{k+1} can be expressed as:

$$\begin{aligned}\phi(t_{k+1}) &= \frac{1}{\lambda}\left[\rho_u^s(t_{k+1}) + cdt_u(t_{k+1}) - cdt^s(t_{k+1})\right] + \\ &\frac{1}{\lambda}\left[-I_\phi(t_{k+1}) + T_\phi(t_{k+1})\right] + N(t_{k+1}) + \varepsilon_\phi(t_{k+1})\end{aligned} \tag{3}$$

The difference between two successive carrier phase measurements at epochs t_{k+1} and t_k can be calculated.

$$\begin{aligned}\Delta\phi &= \phi(t_{k+1}) - \phi(t_k) \\ &= \frac{1}{\lambda}\left(\Delta\rho_u^s + c\Delta dt_u - c\Delta dt^s - \Delta I_\phi + \Delta T_\phi\right) + \Delta\varepsilon_\phi\end{aligned} \tag{4}$$

where Δ represents the differencing operation between two successive epochs. The carrier phase integer ambiguity $N(t_k)$ is equal to $N(t_{k+1})$ when the cycle slip is handled, the difference of the satellite clock bias Δdt^s, the ionospheric delay ΔI_ϕ, and the tropospheric delay ΔT_ϕ vary slowly which approximated at zero. Therefore, the TDCP measurement can be written as:

$$\Delta\phi = \frac{1}{\lambda}\left(\Delta\rho_u^s + c\Delta dt_u\right) + \Delta\varepsilon_\phi \tag{5}$$

The geometric range between the satellite and the receiver antenna can be formulated.

$$\begin{cases}\rho_u^s(t_k) = \boldsymbol{e}(t_k)\cdot\left[\boldsymbol{r}^s(t_k) - \boldsymbol{r}_u(t_k)\right] \\ \rho_u^s(t_{k+1}) = \boldsymbol{e}(t_{k+1})\cdot\left[\boldsymbol{r}^s(t_{k+1}) - \boldsymbol{r}_u(t_{k+1})\right]\end{cases} \tag{6}$$

where $\boldsymbol{r}^s$ is the satellite position, $\boldsymbol{r}_u$ is the receiver position, $\boldsymbol{e}$ is the line-of-sight unit vector from receiver antenna to satellite which can be calculated as:

$$\begin{cases}\boldsymbol{e}(t_k) = \dfrac{\boldsymbol{r}^s(t_k) - \boldsymbol{r}_u(t_k)}{\left\|\boldsymbol{r}^s(t_k) - \boldsymbol{r}_u(t_k)\right\|} \\ \boldsymbol{e}(t_{k+1}) = \dfrac{\boldsymbol{r}^s(t_{k+1}) - \boldsymbol{r}_u(t_{k+1})}{\left\|\boldsymbol{r}^s(t_{k+1}) - \boldsymbol{r}_u(t_{k+1})\right\|}\end{cases} \tag{7}$$

Therefore, the term $\Delta\rho_u^s$ in equation (5) can be expressed as:

$$\begin{aligned}\Delta\rho_u^s &= \rho_u^s(t_{k+1}) - \rho_u^s(t_k) \\ &= \boldsymbol{e}(t_{k+1})\cdot\left[\boldsymbol{r}^s(t_{k+1}) - \boldsymbol{r}_u(t_{k+1})\right] \\ &\quad - \boldsymbol{e}(t_k)\cdot\left[\boldsymbol{r}^s(t_k) - \boldsymbol{r}_u(t_k)\right] \\ &= \left[\boldsymbol{e}(t_{k+1})\cdot\boldsymbol{r}^s(t_{k+1}) - \boldsymbol{e}(t_k)\cdot\boldsymbol{r}^s(t_k)\right] \\ &\quad - \left[\boldsymbol{e}(t_{k+1})\cdot\boldsymbol{r}_u(t_{k+1}) - \boldsymbol{e}(t_k)\cdot\boldsymbol{r}_u(t_k)\right]\end{aligned} \tag{8}$$

Besides, the relationship between the receiver positions at epoch t_{k+1} and epoch t_k can be expressed as:

$$\boldsymbol{r}_u(t_{k+1}) = \boldsymbol{r}_u(t_k) + \Delta\boldsymbol{r}_u \tag{9}$$

where $\Delta\boldsymbol{r}_u$ is the receiver position change between t_k and t_{k+1}.

Substituting equation (9) in (8):

$$\begin{aligned}\Delta\rho_u^s &= \left\{\boldsymbol{e}(t_{k+1})\cdot\boldsymbol{r}^s(t_{k+1}) - \boldsymbol{e}(t_k)\cdot\boldsymbol{r}^s(t_k)\right\} \\ &\quad - \left\{\boldsymbol{e}(t_{k+1})\cdot\left(\boldsymbol{r}_u(t_k) + \Delta\boldsymbol{r}_u\right) - \boldsymbol{e}(t_k)\cdot\boldsymbol{r}_u(t_k)\right\} \\ &= \left\{\boldsymbol{e}(t_{k+1})\cdot\boldsymbol{r}^s(t_{k+1}) - \boldsymbol{e}(t_k)\cdot\boldsymbol{r}^s(t_k)\right\} \\ &\quad - \left\{\boldsymbol{e}(t_{k+1})\cdot\boldsymbol{r}_u(t_k) - \boldsymbol{e}(t_k)\cdot\boldsymbol{r}_u(t_k) + \boldsymbol{e}(t_{k+1})\cdot\Delta\boldsymbol{r}_u\right\}\end{aligned} \tag{10}$$

The equation (5) can be written as:

$$\Delta\phi - \frac{1}{\lambda}\left[\boldsymbol{e}(t_{k+1}) \cdot \boldsymbol{r}^s(t_{k+1}) - \boldsymbol{e}(t_k) \cdot \boldsymbol{r}^s(t_k) \right] + \frac{1}{\lambda}\left[\boldsymbol{e}(t_{k+1}) \cdot \boldsymbol{r}_u(t_k) - \boldsymbol{e}(t_k) \cdot \boldsymbol{r}_u(t_k) \right] = -\frac{1}{\lambda}\boldsymbol{e}(t_{k+1}) \cdot \Delta\boldsymbol{r}_u + \frac{c}{\lambda}\Delta dt_u + \Delta\varepsilon_\phi \quad (11)$$

Let the left part of the equation (11) equal to $\Delta\tilde{\phi}$. Equation (11) can be rewritten in the vector form.

$$\begin{bmatrix} -\boldsymbol{e}(t_{k+1}) & 1 \end{bmatrix} \begin{bmatrix} \Delta\boldsymbol{r}_u \\ c\Delta dt_u \end{bmatrix} = \lambda\Delta\tilde{\phi} - \lambda\Delta\varepsilon_\phi \quad (12)$$

2.2 INS algorithm for displacement increments estimation

The initial attitude can be got by accelerometer leveling and gyroscope compassing. The initial attitude angles including roll, pitch, and azimuth in ENU frame can be written as $[r, p, a]$. Consequently, the initial rotation matrix $\boldsymbol{C}_b^n$ using right-handed system where X is right, Y is forward, and Z is pointing up can be obtained as:

$$\boldsymbol{C}_b^n = \begin{bmatrix} C_{11} & C_{12} & C_{13} \\ C_{21} & C_{22} & C_{23} \\ C_{31} & C_{32} & C_{33} \end{bmatrix} \quad (13)$$

where,

$$\begin{aligned} C_{11} &= \cos a \cos r + \sin a \sin p \sin r \\ C_{12} &= \sin a \cos p \\ C_{13} &= \cos a \sin r - \sin a \sin p \cos r \\ C_{21} &= -\sin a \cos r + \cos a \sin p \sin r \\ C_{22} &= \cos a \cos p \\ C_{23} &= -\sin a \sin r - \cos a \sin p \cos r \\ C_{31} &= -\cos p \sin r \\ C_{32} &= \sin p \\ C_{33} &= \cos p \cos r \end{aligned} \quad (14)$$

The quaternion parameters at t_k can be computed from the rotation matrix $\boldsymbol{C}_b^n$, which can be written as:

$$\begin{bmatrix} q_1(t_k) \\ q_2(t_k) \\ q_3(t_k) \\ q_4(t_k) \end{bmatrix} = \begin{bmatrix} 0.25(C_{32} - C_{23})/q_4(t_k) \\ 0.25(C_{13} - C_{31})/q_4(t_k) \\ 0.25(C_{21} - C_{12})/q_4(t_k) \\ 0.5\sqrt{1 + C_{11} + C_{22} + C_{33}} \end{bmatrix} \quad (15)$$

Due to computational errors, the quaternion parameters should be normalized. The normalized quaternion parameters can be written as:

$$\hat{\boldsymbol{q}} = \boldsymbol{q} \Big/ \sqrt{q_1^2 + q_2^2 + q_3^2 + q_4^2} \quad (16)$$

The rotation matrix $\boldsymbol{C}_b^n$ can be obtained using the quaternion parameters:

$$\boldsymbol{C}_b^n = \begin{bmatrix} \hat{q}_1^2 - \hat{q}_2^2 - \hat{q}_3^2 - \hat{q}_4^2 & 2(\hat{q}_1\hat{q}_2 - \hat{q}_3\hat{q}_4) & 2(\hat{q}_1\hat{q}_3 + \hat{q}_2\hat{q}_4) \\ 2(\hat{q}_1\hat{q}_3 + \hat{q}_2\hat{q}_4) & -\hat{q}_1^2 + \hat{q}_2^2 - \hat{q}_3^2 + \hat{q}_4^2 & 2(\hat{q}_2\hat{q}_3 - \hat{q}_1\hat{q}_4) \\ 2(\hat{q}_1\hat{q}_3 - \hat{q}_2\hat{q}_4) & 2(\hat{q}_2\hat{q}_3 + \hat{q}_1\hat{q}_4) & -\hat{q}_1^2 - \hat{q}_2^2 + \hat{q}_3^2 + \hat{q}_4^2 \end{bmatrix} \quad (17)$$

The correction terms are used to compensate for the Coriolis Effect and can be calculated as:

$$\boldsymbol{\omega}_{in}^b = \boldsymbol{C}_n^b \begin{bmatrix} -\dfrac{\boldsymbol{v}_N}{R_m + h} \\ \dfrac{\boldsymbol{v}_E}{R_n + h} + \boldsymbol{\omega}_{ie} \cos\phi \\ \dfrac{\boldsymbol{v}_E}{R_n + h} \tan\phi + \boldsymbol{\omega}_{ie} \sin\phi \end{bmatrix} \quad (18)$$

where R_m is the meridian radius, R_n is the prime vertical radius, h is the altitude, ϕ is the latitude, $\boldsymbol{v}_E$ is the velocity in East direction, $\boldsymbol{v}_N$ is the velocity in North direction, $\boldsymbol{\omega}_{ie}$ is the angular velocity of the earth rotation. Consequently, the angular changes corresponding to $\boldsymbol{\omega}_{in}^b$ can be determined as:

$$\boldsymbol{\theta}_{in}^b = \boldsymbol{\omega}_{in}^b \cdot \Delta t \quad (19)$$

where is the sampling time interval.

Then the measured angular increments $\boldsymbol{\theta}_{ib}^b$ is compensated for $\boldsymbol{\theta}_{in}^b$ in order to get the actual angular changes of carrier $\boldsymbol{\theta}_{nb}^b$ as follows:

$$\boldsymbol{\theta}_{nb}^b = \boldsymbol{\theta}_{ib}^b - \boldsymbol{\theta}_{in}^b = \begin{bmatrix} \Delta\theta_x \\ \Delta\theta_y \\ \Delta\theta_z \end{bmatrix} \quad (20)$$

The update attitude at t_{k+1} expressed by quaternion can be written as follows:

$$\begin{bmatrix} q_1(t_{k+1}) \\ q_2(t_{k+1}) \\ q_3(t_{k+1}) \\ q_4(t_{k+1}) \end{bmatrix} = \begin{bmatrix} q_1(t_k) \\ q_2(t_k) \\ q_3(t_k) \\ q_4(t_k) \end{bmatrix} + \frac{1}{2} \begin{bmatrix} 0 & \Delta\theta_z & -\Delta\theta_y & \Delta\theta_x \\ -\Delta\theta_z & 0 & \Delta\theta_x & \Delta\theta_y \\ \Delta\theta_y & -\Delta\theta_x & 0 & \Delta\theta_z \\ -\Delta\theta_x & -\Delta\theta_y & -\Delta\theta_z & 0 \end{bmatrix} \begin{bmatrix} q_1(t_k) \\ q_2(t_k) \\ q_3(t_k) \\ q_4(t_k) \end{bmatrix} \quad (21)$$

After normalization, rotation matrix can be computed from the updated quaternion parameters using equation (17).

The velocity increments can be written as:

$$\Delta\boldsymbol{v}^n = \boldsymbol{C}_b^n \cdot \Delta\boldsymbol{v}^b - \left(2\boldsymbol{\Omega}_{ie}^n + 2\boldsymbol{\Omega}_{en}^n\right)\boldsymbol{v}^n \cdot \Delta t + \boldsymbol{g}^n \cdot \Delta t \quad (22)$$

where $\boldsymbol{\Omega}_{ie}^n$ and $\boldsymbol{\Omega}_{en}^n$ represent the skew symmetric matrix corresponding to the angular velocity vector $\boldsymbol{\omega}_{ie}^n$ and $\boldsymbol{\omega}_{en}^n$ respectively, $\boldsymbol{g}^n = \begin{bmatrix} 0 & 0 & -g \end{bmatrix}^{\mathrm{T}}$ represent the normal gravity vector in the navigation frame. $\boldsymbol{C}_b^n \cdot \Delta\boldsymbol{v}^b$ is the measured velocity increments after transformation into the navigation frame, $\left(2\boldsymbol{\Omega}_{ie}^n + 2\boldsymbol{\Omega}_{en}^n\right)\boldsymbol{v}^n \cdot \Delta t$ is the Coriolis correction that compensates for the earth rotation and the navigation frame change of orientation, $\boldsymbol{g}^n \cdot \Delta t$ is the gravity correction.

The update velocity in navigation frame can be computed as:

$$\boldsymbol{v}^n(t_{k+1}) = \boldsymbol{v}^n(t_k) + \frac{1}{2}\left(\Delta\boldsymbol{v}^n(t_k) + \Delta\boldsymbol{v}^n(t_{k+1})\right) \tag{23}$$

The update position including altitude h, latitude ϕ, and λ can be computed as:

$$\begin{cases} h(t_{k+1}) = h(t_k) + \frac{1}{2}\left(v_U(t_{k+1}) + v_U(t_k)\right)\Delta t \\ \phi(t_{k+1}) = \phi(t_k) + \frac{1}{2}\left(\frac{v_N(t_k) + v_N(t_{k+1})}{R_m + h}\right)\Delta t \\ \lambda(t_{k+1}) = \lambda(t_k) + \frac{1}{2}\left(\frac{v_E(t_k) + v_E(t_{k+1})}{(R_n + h)\cos\phi}\right)\Delta t \end{cases} \tag{24}$$

2.3 RTK/INS tightly coupled system

The state vector of RTK/INS tightly coupled system including 9 navigation error states and 6 sensor bias states:

$$\boldsymbol{x} = [\delta\boldsymbol{r}^n \quad \delta\boldsymbol{v}^n \quad \boldsymbol{\phi} \quad \boldsymbol{\varepsilon}^b \quad \boldsymbol{\nabla}^b \quad \delta dt \quad \delta df]^T \tag{25}$$

Where $\delta\boldsymbol{r}^n = [\delta r_E, \delta r_N, \delta r_U]^T$ is the position error vector along the east, north, and upward directions. $\delta\boldsymbol{v}^n = [\delta v_E . \delta v_N, \delta v_U]^T$ is the velocity error vector. $\boldsymbol{\phi} = [\phi_E, \phi_N, \phi_U]^T$ is the misalignment vector. $\boldsymbol{\varepsilon}^b = [\varepsilon_x, \varepsilon_y, \varepsilon_z]^T$ is the gyroscope bias vector. $\boldsymbol{\nabla}^b = [\nabla_x, \nabla_y, \nabla_z]^T$ is the accelerometer bias vector. δdt is the receiver clock error. δdf is the receiver clock drift.

The system dynamic model can be written as

$$\dot{\boldsymbol{x}} = \boldsymbol{F}\boldsymbol{x} + \boldsymbol{G}\boldsymbol{w} \tag{26}$$

where $\boldsymbol{F}$ is the system dynamic matrix, $\boldsymbol{G}$ is the design matrix. $\boldsymbol{w}$ is the process noise.

The measurement model can be written as

$$\begin{bmatrix} \boldsymbol{z}_\rho \\ \boldsymbol{z}_{\dot\rho} \end{bmatrix} = \begin{bmatrix} \boldsymbol{H}_\rho \\ \boldsymbol{H}_{\dot\rho} \end{bmatrix} \boldsymbol{x} + \begin{bmatrix} \boldsymbol{v}_\rho \\ \boldsymbol{v}_{\dot\rho} \end{bmatrix} \tag{27}$$

And it can be written simply as

$$\boldsymbol{z} = \boldsymbol{H}\boldsymbol{x} + \boldsymbol{v} \tag{28}$$

Where ρ represents the pseudorange observation. $\dot\rho$ represents the pseudorange rate observation. $\boldsymbol{z}$ is the measurement vector. $\boldsymbol{H}$ is the design matrix. $\boldsymbol{v}$ is the measurement noise.

Kalman filter is used to estimate the state vector. The time update can be written as

$$\hat{\boldsymbol{x}}_{k|k+1} = \boldsymbol{\Phi}_{k,k-1}\hat{\boldsymbol{x}}_{k-1} \tag{29}$$

$$\boldsymbol{P}_{k|k+1} = \boldsymbol{\Phi}_{k,k-1}\boldsymbol{P}_{k-1}\boldsymbol{\Phi}_{k,k-1}^T + \boldsymbol{\Gamma}_{k-1}\boldsymbol{Q}_{k-1}\boldsymbol{\Gamma}_{k-1}^T \tag{30}$$

The measurement update can be written as

$$\boldsymbol{K}_k = \boldsymbol{P}_{k|k-1}\boldsymbol{H}_k^T\left(\boldsymbol{H}_k\boldsymbol{P}_{k|k-1}\boldsymbol{H}_k^T + \boldsymbol{R}_k\right)^{-1} \tag{31}$$

$$\boldsymbol{x}_k = \hat{\boldsymbol{x}}_{k|k+1} + \boldsymbol{K}_k\left(\boldsymbol{Z}_k - \boldsymbol{H}_k\hat{\boldsymbol{x}}_{k|k+1}\right) \tag{32}$$

$$\boldsymbol{P}_k = (\boldsymbol{I} - \boldsymbol{K}_k\boldsymbol{H}_k)\boldsymbol{P}_{k|k-1}(\boldsymbol{I} - \boldsymbol{K}_k\boldsymbol{H}_k)^T + \boldsymbol{K}_k\boldsymbol{R}_k\boldsymbol{K}_k^T \tag{33}$$

3. Test and Results

In the test, numerical analysis is conducted using a dataset provided with the GINav library (Chen et al., 2021). This vehicle based, driving dataset was collected in a suburban environment. A Trimble R10 receiver is used to collect GNSS measurements. The Inertial Measurement Unit (IMU) measurements are collected from a tactical grade sensor. The NovAtel SPAN-CPT system provides accurate solutions as the ground truth (GT). Figure 1 shows the number of visible satellites from GPS, Galileo, and Beidou constellations in test period for 30 minutes plotted by rtkplot (Takasu and Yasuda, 2009). There are 7 to 14 available satellites that can be stable used in RTK/INS tightly coupled system during the test shown in Figure 2.

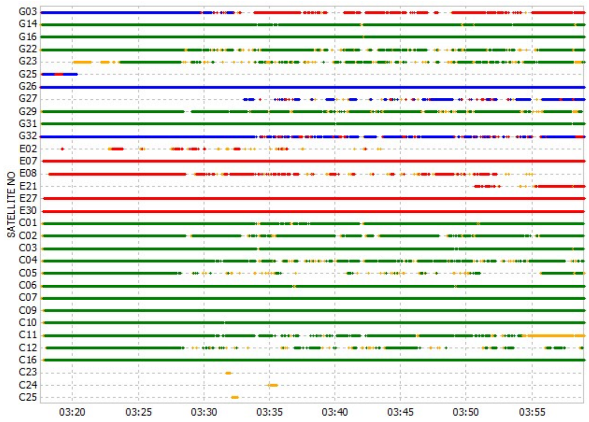

Figure 1. The number of visible satellites during test.

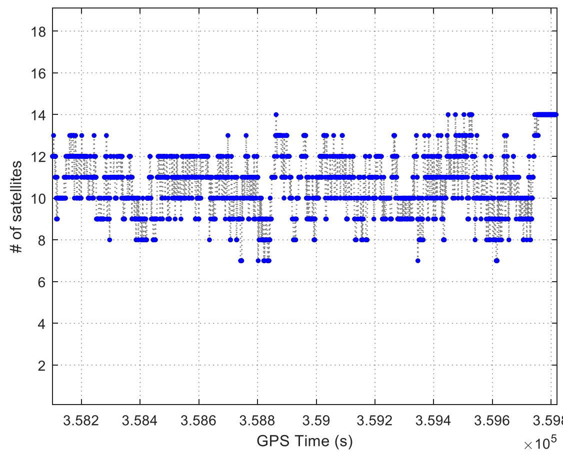

Figure 2. The number of satellites used in RTK/INS tightly coupled system.

Figure 3. is the sky-plot of visible satellites during the test for 30 min. There are more than 17 satellites elevation angles consistently greater than 15 degrees during the test. The geometric distribution of visible satellites is even in terms of elevation, which is beneficial for positioning.

The horizontal trajectory of the vehicle in the East-North plane during the test is presented in Figure 4. As shown in the figure, the trajectory forms two complete circular loops, total of approximately 30 minutes. This long-term test was intentionally designed to verify the accuracy of the system's positional tracking capabilities.

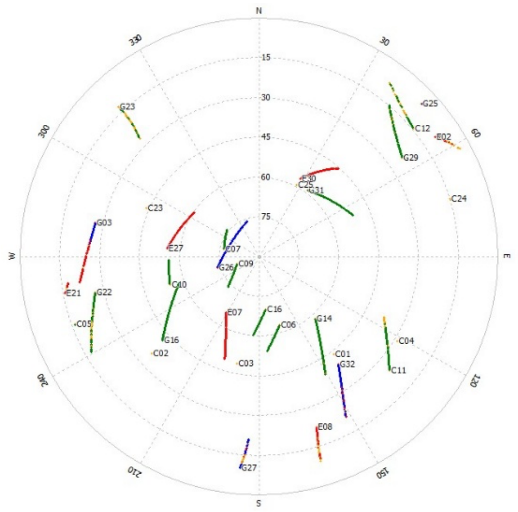

Figure 3. The sky-plot of visible satellites.

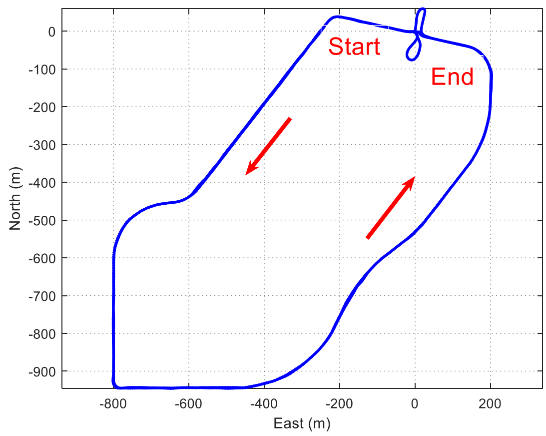

Figure 4. Horizontal trajectory in the test.

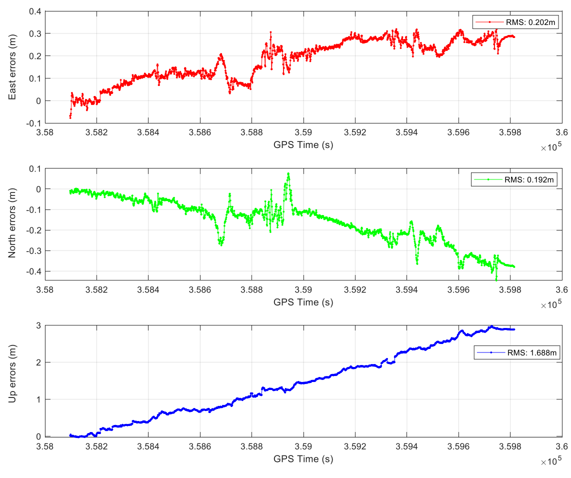

Figure 5. Positioning errors of TDCP.

The positioning errors of TDCP in East, North, and Up directions are shown in Figure 5. After providing an initial position by RTK/INS tightly coupled system, TDCP can get high-precision position and its error exhibited a gradual drift over the 30 minutes test duration, as expected due to the accumulation of displacement error. However, despite this drift, the positioning error remained within relatively acceptable bounds for general navigation scenarios. The maximum errors over 30 minutes in east, north, and up direction are around 0.333 m, -0.446 m, and 3.598 m, respectively. Over short time spans, the TDCP solution maintained high accuracy, but over extended periods, the accumulated drift became noticeable, highlighting the need for periodic error correction or integration with additional sensors for long-duration applications. In addition, the Up-position errors show the largest error drifting over time mainly due to the poorer geometric distribution of the visible satellites in vertical direction than that in horizontal.

Although TDCP error remains relatively small, its cumulative effect over time prevents the system from achieving high-precision positioning. To mitigate this issue, periodic error correction must be applied, through external aiding sources. RTK/INS tightly coupled system is applied to correct the error. The positioning errors of TDCP with correction by RTK/INS tightly coupled algorithm at a 5-minute cycle, 10-minute cycle, and 15-minute cycle are illustrated in Figure 6, Figure 7, and Figure 8, respectively. As noted in purple rectangle in Figure 6, the accumulation errors of TDCP at the end of 5th minute reach to 0.144 m, -0.051 m, and 0.596 m in East, North, and Up directions, respectively. Then RTK/INS tightly coupled algorithms correct the errors to 0.034 m, approximately 0 m, and 0.012 m, respectively. Other calibration points have the same error correction effect. Especially in Figure 8, RTK/INS tightly coupled algorithms correct the accumulation error of 20-minute TDCP drifting significantly. the accumulation errors of TDCP at the end of 20th minute reach to 0.219 m, -0.116 m, and 1.496 m in East, North, and Up directions, respectively. Then RTK/INS tightly coupled algorithms correct the errors to -0.011 m, -0.011 m, and -0.017 m, respectively.

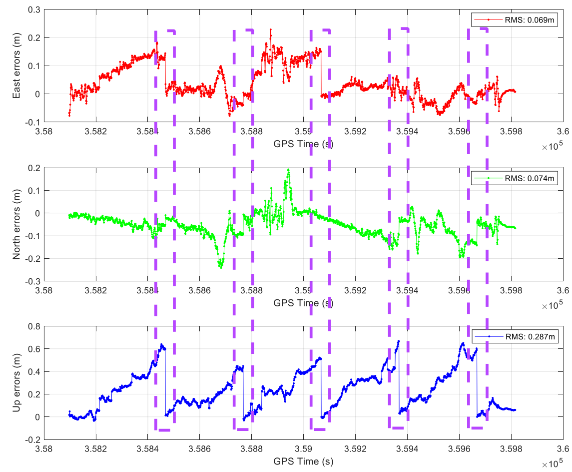

Figure 6. Positioning errors of TDCP with correction by RTK/INS tightly coupled system at a 5-minute cycle.

Proceedings of the International Cartographic Association, 7, 23, 2025 | https://doi.org/10.5194/ica-proc-7-23-2025
32nd International Cartographic Conference (ICC 2025), 17–22 August 2025, Vancouver, Canada.
This contribution underwent single-blind peer review based on submitted abstracts.

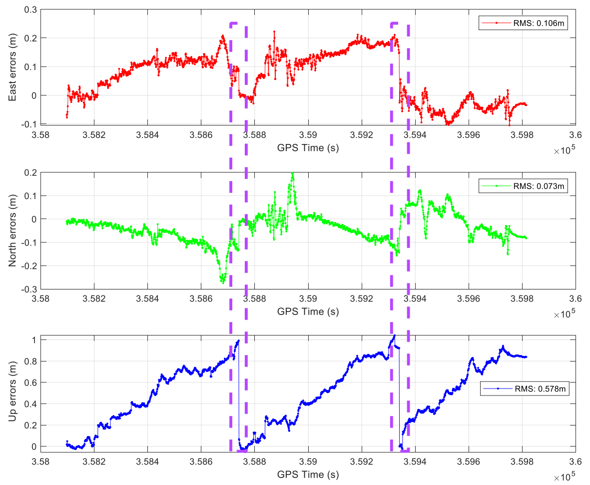

Figure 7. Positioning errors of TDCP with correction by RTK/INS tightly coupled system at a 10-minute cycle.

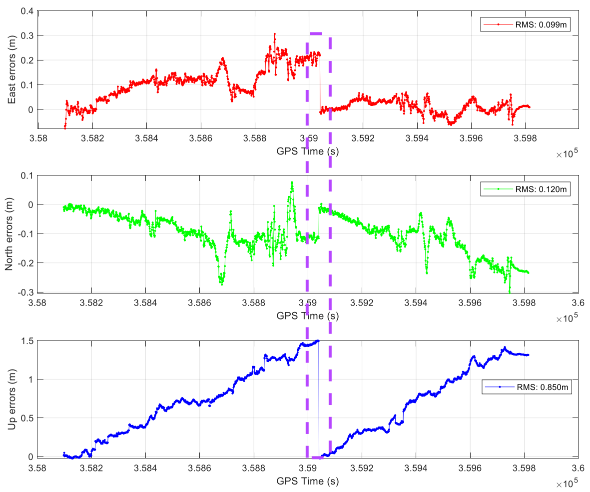

Figure 8. Positioning errors of TDCP with correction by RTK/INS tightly coupled system at a 15-minute cycle.

Table 1. RMS of positioning errors of TDCP, and TDCP with correction.

Methods	Correction cycle (minutes)	RMS of positioning errors (m)		
		East	North	Up
TDCP without correction		0.202	0.192	1.688
TDCP with correction	5	0.069	0.074	0.287
	10	0.106	0.073	0.578
	15	0.099	0.120	0.850

By incorporating periodic corrections, the system can reset its error accumulation, significantly improving positioning accuracy. This approach is particularly beneficial for long-duration operations, which adaptive correction intervals triggered by time thresholds can further optimize performance, ensuring that corrections are applied only when necessary. For the complexity of RTK/INS tightly coupled algorithm is much more than TDCP, TDCP-based navigation systems can reduce computational burden and power consumption. The periodic correction can help system maintain relative high precision positioning.

The RMS of positioning errors of TDCP without-, and with-correction for 30 minutes are shown in Table 1. RMS significantly decreases with calibration by RTK/INS tightly coupled system compared to cases without calibration, which demonstrates the effectiveness of periodic correction in mitigating cumulative drift for TDCP. The most notable improvement occurs in up direction with the highest error (1.688 m), where correction reduces the deviation by approximately 1.401 m, highlighting its critical role in enhancing long-duration positioning reliability. Although theoretically, reducing the cycle time can decrease the RMS, comparing the TDCP results of 5-minute cycle correction, 10-minute cycle correction, and 15-minute cycle correction, the reduction of cycle time cannot decrease RMS in all directions. Therefore, a proper cycle should be set considering power consumption and performance in practical work.

4. Conclusions

In this paper, we develop a tightly coupled RTK/INS-aided TDCP navigation system to reduce power assumption while maintain high positioning precision for autonomous vehicles in challenging environments. The proposed system leverages the complementary strengths of RTK/INS, and TDCP to mitigate the limitations of standalone TDCP navigation, particularly its susceptibility to cumulative error drift over time. Experimental results demonstrate significant improvements in positioning precision across all three coordinate directions. These enhancements are achieved through periodic correction, which effectively suppress the drift in TDCP positioning. While TDCP alone provides reasonably accurate positioning for short durations, the results confirm that integrating RTK/INS aiding and periodic correction substantially refines long-term performance. The proposed system not only improves positioning consistency but also promotes energy-efficient navigation by minimizing the computational. Future work could explore adaptive correction intervals to further optimize accuracy and resource usage.

5. Acknowledgements

The financial support from the Chinese Scholarship Council (CSC) are greatly acknowledged.

6. References

Van Brummelen, J., O'brien, M., Gruyer, D. and Najjaran, H., 2018. Autonomous vehicle perception: The technology of today and tomorrow. *Transportation research part C: emerging technologies*, vol. *89*, pp.384-406. doi: doi.org/10.1016/j.trc.2018.02.012Get rights and content.

Hegarty, C.J. and Chatre, E., 2009. Evolution of the global navigation satellitesystem (gnss). *Proceedings of the IEEE*, *96*(12), pp.1902-1917. doi: 10.1109/JPROC.2008.2006090.

Zeybek, M., 2021. Accuracy assessment of direct georeferencing UAV images with onboard global navigation satellite system and comparison of CORS/RTK surveying methods. *Measurement Science and Technology*, 32(6), p.065402. doi: 10.1088/1361-6501/abf25d.

Feng, Y. and Wang, J., 2008. GPS RTK performance characteristics and analysis. *Positioning*, *1*(13). https://www.scirp.org/html/376.html.

Tokura, H., Kubo, N., Effective Satellite Selection Methods for RTK-GNSS NLOS Exclusion in Dense Urban Environments, In: *Proc. of the 29th International Technical Meeting of the Satellite Division of The Institute of Navigation (ION GNSS+ 2016)*, Portland, Oregon, September 2016, pp. 304-312. doi: doi.org/10.33012/2016.14801.

Soon, B.K., Scheding, S., Lee, H.K., Lee, H.K. and Durrant-Whyte, H., 2008. An approach to aid INS using time-differenced GPS carrier phase (TDCP) measurements. *Gps Solutions*, *12*, pp.261-271. doi: doi.org/10.1007/s10291-007-0083-7.

Li, Z., Zhu, N. and Renaudin, V., 2022, June. Velocity protection level for wearable devices on TDCP-based pedestrian navigation. In: *Proc. 2022 International Conference on Localization and GNSS (ICL-GNSS)* pp. 01-07. doi: 10.1109/ICL-GNSS54081.2022.9797022.

Suzuki, T., 2022. GNSS odometry: Precise trajectory estimation based on carrier phase cycle slip estimation. *IEEE Robotics and Automation Letters*, *7*(3), pp.7319-7326. doi: 10.1109/LRA.2022.3182795

Chen, K., Chang, G. and Chen, C., 2021. GINav: A MATLAB-based software for the data processing and analysis of a GNSS/INS integrated navigation system. *GPS solutions*, *25*(3), p.108. doi: doi.org/10.1007/s10291-021-01144-9.

Takasu, T. and Yasuda, A., 2009, November. Development of the low-cost RTK-GPS receiver with an open source program package RTKLIB. *In International symposium on GPS/GNSS*, Vol. 1, pp. 1-6. doi: doi.org/10.1007/s10291-021-01144-9.